EUROfusion

EUROFUSION WPDTT2-PR(16) 16378

R Zagorski et al.

The DTT device: power and particle exhaust

Preprint of Paper to be submitted for publication in
Fusion Engineering and Design

This work has been carried out within the framework of the EUROfusion Consortium and has received funding from the Euratom research and training programme 2014-2018 under grant agreement No 633053. The views and opinions expressed herein do not necessarily reflect those of the European Commission.

The DTT device: power and particle exhaust

R. Zagórski[1], V. Pericoli Ridolfini[1,2], F.Subba[3], F.Crisanti[2], G.Giruzzi[4], H.Reimerdes[5]

[1]*Institute of Plasma Physics and Laser Microfusion, 01-497 Warsaw, Poland*
[2]*Politecnico di Torino, Italy*
[3]*ENEA-Frascati, Via E. Fermi 45, 00044 Frascati Italy*
[4]*CEA, DRFC/CEA/Cadarache, 13108 St. Paul-lez-Durance, France*
[5]*Ecole Polytechnique Federale de Lausanne, Centre de Recherches en Physique des Plasmas,Suisse, 1015 Lausanne, Switzerland,*

Abstract

The possible scenarios at full power of the DTT device with standard (SD) and quasi snow flake (QSF) divertor configurations have been analysed for the aspect of safely handling the power to be exhausted on the divertor targets. In this conceptual design phase the computational tools have been chosen mainly on the basis of their simplicity and rapidity. The code COREDIV was used for a preliminary self-consistent description of the coupled edge-core system. Subsequently, a more punctual analysis has been carried out on the SOL with the TECXY code. COREDIV results, show that operations without impurity seeding may be problematic in all scenarios, and especially at the higher densities where tungsten is virtually absent in the core and the core radiation very low.

The main outcome of this study is that in term of global parameters little difference exists between the two configurations for low working densities. The reason is identified in the fact that the topology modifications occur in region where the dissipative processes, radiation inelastic collisions etc., are rather negligible to be enhanced at significant level.
The situation shows different at higher density where the QSF seems indeed to favour detached operations and strongly radiating regimes. This trend is reinforced by lowering the power entering the SOL and by faster cross-field diffusion. These very important regimes seem to be reachable by the advanced configurations of DTT, for some appropriate choice of the working parameters.

1. Power and particle exhaust in DTT

The problem of controlling and safely managing the power exhaust is one of major tasks of the DTT device. It has therefore started the exploration of the divertor operating conditions with modelling tools able to produce in this phase of the project meaningful results in a reasonable lapse of time. Clearly this implies using codes simpler than the most sophisticated ones presently available in the scientific community. Nevertheless the produced overview should outline the peculiarities, if any, of the DTT operating scenarios and provide sound inputs for a subsequent more complex analysis. Furthermore the plasma and device details necessary for a rigorous simulation are still not completely defined.

The first step has been to analyse the general plasma performance by means of the system code METIS and check the consistency of the results with the scrape-off layer (SOL) status through a relatively simple code (0D in the core, two points model for the SOL). The subsequent step has been to use this information for validating and detailing the scenario with the COREDIV code [1], which couples the 1D plasma transport in the core and 2D multi-fluid transport in the SOL. In this code the coupling SOL-core is given by imposing the continuity of energy and particle fluxes, densities and temperatures at the separatrix, and by using the computed fluxes from the core as boundary conditions for the SOL. In turn, the

temperatures and densities calculated in the SOL are used as boundary conditions for the core module. In the core, the 1D radial transport equations for bulk ions, for each ionization state of impurity ions and for the electron and ion temperature are solved. All ions have the same temperature. Line radiation and bremsstrahlung determine the energy losses. Neoclassical transport is considered in the bulk, with a contribution from anomalous transport that is scaled to reproduce the prescribed energy confinement, which is assumed being the ITER-98y2 ELMy H-mode scaling [2] in the present calculations. The plasma density profile is given by the solution of the radial diffusion equation. The source intensity is determined by the internal iteration procedure in such a way that the average electron density obtained from neutrality condition equals that of the scenario considered. The impurity transport is described by the standard neoclassical (collisionality dependent) and anomalous transport. The anomalous impurity transport includes only a diffusive term, since the anomalous pinch velocity is set to zero.

The 2D multi-fluid model in the SOL and divertor region is based on Braginskij-like equations [1] for the background plasma and rate equations for the ionization state of each impurity species. These latter can be both added and intrinsic, i.e. sputtered from the target plates. The various ion species in their different charge states are treated as separate fluids but all at the same temperature T_i, distinct from that of the electron fluid, T_e. The continuity, parallel momentum and energy equations are solved. For the neutrals an analytical description is assumed with an assigned recycling coefficient. The transport along field lines is assumed to be classical and transport coefficients follow from the 21-moment Grad approximation. The parallel velocities and the gradients of densities and temperatures are assumed to be zero at the midplane (stagnation point). The radial transport is anomalous with prescribed radial transport coefficients ($D_\perp$=0.5 m^2/s, $\chi_{e\perp}$=1.0 m^2/s, $\chi_{i\perp}$=0.5 m^2/s). They give the heat flux e-folding length of the order of 1 cm. However since the SOL is modelled by a simple slab geometry (poloidal and radial directions) that neglects both the real divertor geometry and a possible flux expansion at the plate, only the total divertor load is here considered, not its distribution along the target. The standard sheath boundary conditions are imposed at the plates and the plasma is assumed to be in the attached mode.

The main limitations of this modelling can be identified in the lack of pedestals, in the missing drifts and in the absence of the impurity anomalous pinch. A temperature pedestal may lead to a broadening of the radiation zone inside the separatrix. The effect of the drifts would be concentrated in the SOL and in the boundary region close to the separatrix, where they might affect transport significantly, due to their interrelation with the radial electric field and its shear. Nevertheless the absence of drifts in COREDIV does not lead to a significant loss of generality of our results since their influence on the core contamination and on the global energy balance of the relatively high density plasmas is expected to be rather small. Moreover the high magnetic field in DTT (<6.5 T) would tend to suppress the drifts effects. Conversely, the anomalous pinch velocity, possible when internal transport barriers develop, can significantly affect the high Z impurity density profile.

Both in the core and in the SOL therefore the impurity fluxes and the associated radiation losses are calculated fully self-consistently, as well as the energy losses due to interactions with hydrogenic atoms (line radiation, ionization and charge exchange).

The target material is assumed to be tungsten. The additional impurities considered in these first simulations to mitigate the thermal loads are N or Ar, puffed from the divertor region.

Validation of the COREDIV code comes from the successful simulations of N and Ne seeded JET discharges [3]. Runs also for ITER scenarios with injected impurities have been carried out [4], as well as for the projected tokamak FAST [5].

Three different volume averaged densities have been considered: the reference one, $\langle n_e \rangle_{ref}$, one lower $\langle n_e \rangle_{low}$, and one higher, $\langle n_e \rangle_{high}$, respectively =1.8, 1.0, 2.5×10^{20} m^{-3} with a correspondent density at the separatrix of 0.74, 0.49 1.0×10^{20} m^{-3}. Constant have been kept the macroscopic parameters, plasma current, magnetic field and auxiliary power, respectively: I_p = 6.0 MA; B_T =6.0 T ; P_{aux}= 40 MW. The outputs are given below in table I, II, III

Table I - COREDIV results for $\langle n_e \rangle_{ref}=1.8\times10^{20}$ m^{-3}; $n_{e,sep}=7.4\times10^{19}$ m^{-3}

	W only	W+N - I	W+N II	W+Ar
$\Gamma_{puff,Z}$ (10^{20} s^{-1})	/	5	20	1
$Z_{eff,0}$	1.02	1.29	1.51	1.45
T_{e0} (keV)	12.8	13.8	14.6	14.6
n_W (%)	5.2×10^{-4}	7.5×10^{-3}	1.0×10^{-2}	1.0×10^{-2}
$n_{Ar,N}$ (%)	0	8.3×10^{-2}	0.41	3.35×10^{-2}
$f_{rad,tot}$ (%)	12.3	44.7	62.1	61.7
P_{SOL} (MW)	36.7	24.7	19.4	18.5
P_{plate} (MW)	32.0	19.6	12.7	12.8
$f_{loss,SOL}$ (%)	12.9	20.8	34.5	30.6
$T_{e,sep}$(eV)	210	178	161	157
$n_{e,plate}$ (10^{19} m^{-3})	39.7	58.4	67.8	64
T_{plate} (eV)	29.6	14.5	6.8	7.2

As compared with the calculations performed for FAST [5] with P_{aux}=40 MW we see that the loads are slightly increased mostly because of the smaller working density. This increment is however balanced by the larger major radius if the specific loads are concerned. Therefore similar warnings apply about the risk of no impurity seeding.

Table II - COREDIV results for $\langle n_e \rangle_{low}=1.0\times10^{20}$ m^{-3}; $n_{e,sep}=4.9\times10^{19}$ m^{-3}

	W only	W+N - I	W+N II	W+Ar I	W+Ar II
$\Gamma_{puff,Z}$ (10^{20} s^{-1})	/	5	10	1	2
$\Gamma_{p,SOL}$ (10^{21} s^{-1})	1.82	1.59	1.43	1.28	1.18
$Z_{eff,0}$	1.59	2.17	2.56	2.89	3.46
T_{e0} (keV)	19.2	19.91	20.65	21.6	22.5
n_W (%)	0.017	0.032	0.04	0.047	0.049
$n_{Ar,N}$ (%)	0	0.15	0.356	0.072	0.24
$f_{rad,tot}$ (%)	22.5	39.7	52.4	65.3	74.2
P_{SOL} (MW)	32.4	26.1	21.5	16.4	13.9
P_{plate} (MW)	28.7	22.2	17.3	12.13	8.6
$f_{loss,SOL}$ (%)	11.7	15.1	19.7	26.2	38.2
$T_{e,sep}$(eV)	218	194	176	152	140
$n_{e,plate}$ (10^{19} m^{-3})	16.6	22.3	28.8	33.5	41.3
T_{plate} (eV)	57.8	33.2	21.9	13.8	8

Table III - COREDIV results for $\langle n_e \rangle_{high}=2.5\times10^{20}$ m^{-3}; $n_{e,sep}=1.\times10^{20}$ m^{-3}

	W only	W+N - I	W+N II	W+Ar I
$\Gamma_{puff,Z}$ (10^{20} s^{-1})	/	3	5	3
$\Gamma_{p,SOL}$ (10^{21} s^{-1})	5.1	4.74	4.62	4.1
$Z_{eff,0}$	1	1.05	1.07	1.25

T_{e0} (keV)	11.02	11.3	11.4	12
n_W (%)	0	0.001	0.001	0.002
$n_{Ar,N}$ (%)	0	0.032	0.054	0.056
$f_{rad,tot}$ (%)	18.2	30.8	35.2	55.7
P_{SOL} (MW)	36.8	32.4	30.9	25.3
P_{plate} (MW)	28.5	23.5	21.7	12.9
$f_{loss,SOL}$ (%)	22.5	27.5	29.9	48.8
$T_{e,sep}$(eV)	185	176	173	159
$n_{e,plate}$ (10^{19} m^{-3})	104	109	111	119
T_{plate} (eV)	9.4	6.4	5.7	3.1

A preliminary selection of the acceptable scenarios from the heat load point of view can be made from the following simple arguments on the expected width of the power flow channel in the outboard equator Δ_{eq}. According to the present scaling law [6], $\Delta_{eq}\approx 4$ mm is a reasonable value for DTT if we add the effect of the diffusion into the divertor private region that COREDIV neglects. Assuming a flux expansion by 5 times onto the target, usual for a conventional standard divertor (SD) configuration, we get at target $\Delta_{target}= 2$ cm, which in turn can rises up to $\Delta_{target}\approx 6$ cm, due to the target tilting, corresponding to a strike angle for the poloidal field ≈20°, value hard to be further lowered. If the maximum safe load is taken as $P_L=15$ MW/m^2 and the load is equally shared between the two plates, we get the maximum acceptable power on plates $P_{max}=2\times P_L\times\Delta_{target}\times(2\pi R)=23.7$ MW for the major radius of the device R=2.1 m.

2. 2D edge simulations with TECXY

The above tables suggest that operations without impurity seeding may be problematic in all scenarios, and especially at the higher densities where tungsten is virtually absent in the core and the core radiation very low. In the reference scenario a small puff rate of either Ar or N will permit operations at $Z_{eff}\leq 1.5$. At low density a higher Z_{eff} (>2.5) should be accepted for a safe operation, whereas at the highest density the Ar or N injection rates so far considered seem still too poor. This analysis therefore depicts a rather border-line situation if we want to limit the impurity seeding, in order to have the figure of merit P_{SOL}/R close to, and possibly higher than, the ITER value. Consequently, a more detailed analysis, limited to pure D_2 plasma for the reasons just given has been carried out with a dedicated 2D transport edge code, namely TECXY [7]. This code is particularly useful in this phase of the project since it allows a rather wide exploration of the operating parameter space faster than other more complex codes, as EDGED2D, SOLPS or SOLEDGE. The main reason is the simple analytical treatment of the neutral dynamics instead of the Monte Carlo technique. All the other main physical features are the same as for the other codes. The actual magnetic topology is taken into account whereas the divertor geometry is simplified with target perpendicular to the poloidal field B_{pol}. This indeed has negligible effect within the analytical neutral model, contrarily to the Monte Carlo case, and avoids, on the other hand, to distort the computing mesh close to targets. Preserving the ideal cell form with two sides perpendicular and two parallel to B_{pol} allows solving more accurately the differential equations. The actual fluxes are recovered simply by multiplying the output by $\sin\alpha_t$, being α_t the angle between B_{pol} and the local poloidal target trace. Furthermore a reliable analysis with the more complex codes would require knowing the detailed design of the divertor, namely shape of the plates, pumps, baffles, etc., which instead is still missing.

In this phase we consider only the standard and extended divertor (sometimes called also quasi snow flake (QSF)) configurations, SD and XD respectively. The two mentioned

configurations are sketched in Figure 1 (full poloidal section) and Figure 2 (zoom on the divertor region). In XD two secondary nulls of B_{pol} external to the main vessel are added on both the inner and outer divertor leg. For this latter this X point is clearly visible in Figure 1 (right frame). Consequently, the poloidal flux is expanded, as evidenced by comparing the right with the left side of Figure 2. Because of the still undefined divertor shape a very rough wall boundary is assumed for both configurations, the green line in the mentioned figures. Consequently, only a relative comparison can be done between the two configurations, the absolute values being meaningless at this stage. The target position is assumed to be located just at the end of the flux lines shown in Figure 2. The corresponding flux expansions at the inner and outer target (IT, OT) - ratio between the distance of two adjacent flux surfaces at the target and at the outer equator - are plotted in Figure 3 versus the outer equatorial distance from the separatrix.
Actually other configurations have been developed for DTT, as double null (DN), the SF minus and SF plus together with their variants distinguishing for extension, shape and depth of the B_{pol} null region in between the X points. Here we fix our attention on the XD configuration since it shows as a promising tool for mitigating the target heat loads, still maintaining a high degree of compatibility for divertor design in common with SD. This mitigation has been found in a recent preliminary experiment on the EAST tokamak and has successfully been reproduced by TECXY [8] . Strong XD mitigating properties have also been found in previous modelling studies for the proposed FAST tokamak [9] and for the planned EAST scenarios [8]. These papers also show that QSF not only spreads the load over a larger surface, but could also induce a significant increase of the volume power losses inside the SOL, consequent to the increase of the total connection length L_c of the magnetic field lines. This is in turn caused by their enhanced toroidal twist due to the lower poloidal field mainly in the divertor region, as the larger flux expansion attests. The longer L_c, and hence of the particle dwell time, favour the dissipative inter-particle interactions.
In the present case comparison of the connection lengths between XD and SD is presented in Figure 4 versus the outer equatorial distance from the separatrix for both the divertor legs. The length is calculated form the target position to the main X point

Main assumptions for the code inputs

The exploration of the operating parameters has been carried out by performing a density scan on the value at the stagnation point onto the separatrix, $n_{e,s}$. Stagnation is defined as the symmetry point where the fluid velocity is 0 and has opposite directions on either side. The scan is carried out between approximately $0.5 \leq n_{e,s} \leq 1.3\times10^{20}$ m^{-3} for each of the three selected couples of values of $(D_\perp, \chi_\perp)$ = (0.10, 0.25) – (0.15, 0.35) – (0.50, 0.50) m^2/s, being $D_\perp$ and $\chi_\perp$ the cross-field diffusion coefficients respectively of particles and heat (both electrons and ions). These three couples give an upstream e-folding decay length $\lambda_{q\parallel,u.s}$= 2, 3, 4 mm for the cross-field profile of the quantity $n_e\times T_e^{3/2}$, shown for the SD reference case in Figure 5. This quantity indeed best approximates the power flow channel width when the parallel temperature gradient, and conductive heat transport with it, is negligible. These values of $\lambda_{q\parallel,u.s}$ must be compared with the value ≥2.5 mm for the width inside the divertor, mapped at the outer midplane, given by the empirical scaling laws for DTT [10]. The uncertainty depends on the specific design of the divertor, which is still missing. Possibility to reach 3 mm is not to be excluded. This value also is consistent with a width resulting from the length of the poloidal ion gyro radius (≈ 2mm) + diffusion into the private region, which is neglected in the present TECXY simulations. Clearly, different single values for $D_\perp$ and $\chi_\perp$ can produce the same $\lambda_{q\parallel,u.s}$ and also originate different profiles of n_e and T_e.

The above density scans are fully repeated for the maximum foreseen power crossing the separatrix namely P_{SOL}=35 MW and for a bit less value, namely P_{SOL}=25 MW, giving for the figure of merit P/R the respective values of ≈16 and ≈12 MW/m.

QSF versus SD heat loads for the reference standard scenario

As far as the global quantities are concerned the situation is depicted in Figure 6. Here we compare the fraction of the total volume losses versus the upstream plasma density at separatrix for the cases with P_{SOL}=35 and 25 MW, respectively on the left and right column. The three frames on each column refer to the three mentioned couples of cross-field diffusion coefficients, sorted from the top on increasing values of $\lambda_{q||,u.s}$.
Comparing the left versus the right column, it is evident how larger power fraction are lost for the lower power case, as a consequence of the lower temperatures, on average, that enhance all the volume losses processes, mostly charge exchange and D line radiation. The increase of the cross section for these processes has also the positive feedback to increase the number of neutrals, i.e. of the centres for the dissipative processes.
Running along one column it appears that the equivalence between the two configurations can be broken, with a sudden increase of the power loss for QSF, for sufficiently long $\lambda_{q||,u.s}$. This is a strong indication of start of, or at least of conditions very close to, detachment. This occurs earlier in density for the lower P_{SOL} case, for which it appears possible for the density range attainable by DTT even for the case $\lambda_{q||,u.s}$=3 mm that is more frequently assumed as reference. To this purpose we note that for a given average core density it is very likely that the QSF attains actual higher separatrix density than SD, because of the longer L_{con}. This is expected on the basis of both the experimental results on FTU [11] and the present simulations, which require less particle flux leaving the core for QSF for the same $n_{e,sep}$.
The mitigations that are obtained in the different situations are plotted in Figure 7, as the ratio of the peak value to the lowest density SD case. In the left (right) column there is the case with P_{SOL}=35 (25) MW, in the upper (lower) frame there is inner (outer) target. The mitigation required for a sustainable load of 15 MW/m^2 is given for reference as a horizontal green line. We recall, however, that this are loads on target set perpendicular to B_{pol} and therefore are an upper limit to the load, whose actual value is subjected to the real target positioning. The mitigation with XD is always much larger on the outer target than on the inner one, where even an increase with respect to SN can be found. This is the result of the less expansion on IT and of the fact the longer connection lengths shift the stagnation point towards the OT and then the total power conveyed to the IT increases. Neglecting the effect of the plate tilting, for P_{SOL}=35 MW the load is hardly sustainable on the inner target for both configurations, whereas for OT it is again very hard for SD but becomes sustainable at moderate values of $n_{e,sep}$ for QSF. For P_{SOL}=25 MW the sustainability is much easier except for OT, SD case. For this value of P_{SOL} also the transition to detached case for QSF are well recognized, by a sudden drop of the load that occurs on both targets almost simultaneously
The reason why there is a large drop in the OT for QSF case are not only due to the flux expansion, but in large part also to the different width of the power flowing channel in terms of flux coordinates that is induced by the increase of the connection lengths. This is evidenced in Figure 8 where the deposition profiles normalized to the peak value are plotted versus the outer equator SOL depth, in order get rid of flux expansion effect. A well attached case with the same volume power loss is considered. The QSF channel width is much wider than SD in term of poloidal flux coordinate for the OT, whereas it is negligibly different for the IT. The corresponding density and temperature profiles are shown in Figure 9 for the OT only. Density is normalized to its peak value. Clearly the spreading of the power is due to the temperature spreading. Density adjusts its value in order to keep the pressure balance along the flux line. The main reason for this large T_e radial broadening is at present believed being

caused by a significant variation occurring in the conductive parallel transport. Indeed according to the simple two point model [12], the increase of the connection length introduces changes in the upstream and target temperatures. The possible decrease of the target temperature and also of the average value along the flux tube can drop significantly the parallel conductivity. In addition, the longer length can also decrease the parallel T_e gradient along the real flux tube that further slows down the energy transport. Consequently the flow channel width must expand to ensure the same total transport rate. In support of this view Figure 10 compares the behaviour of the temperature at the separatrix for SD and QSF as a function of the poloidal distance from the main X point. The temperature drop to the OT is quite evident QSF. We also remind that the actual flux tube lengths are quite different, despite the same poloidal length, as can be seen from Figure 4. At present this is still a qualitative explanation. A more punctual analysis is ongoing. The modified sharing of the power between the inner and outer legs should also affect this change. A power increase tends to hinder this change, as it apparently happens for the inner target, a decrease instead tends to favour the change.

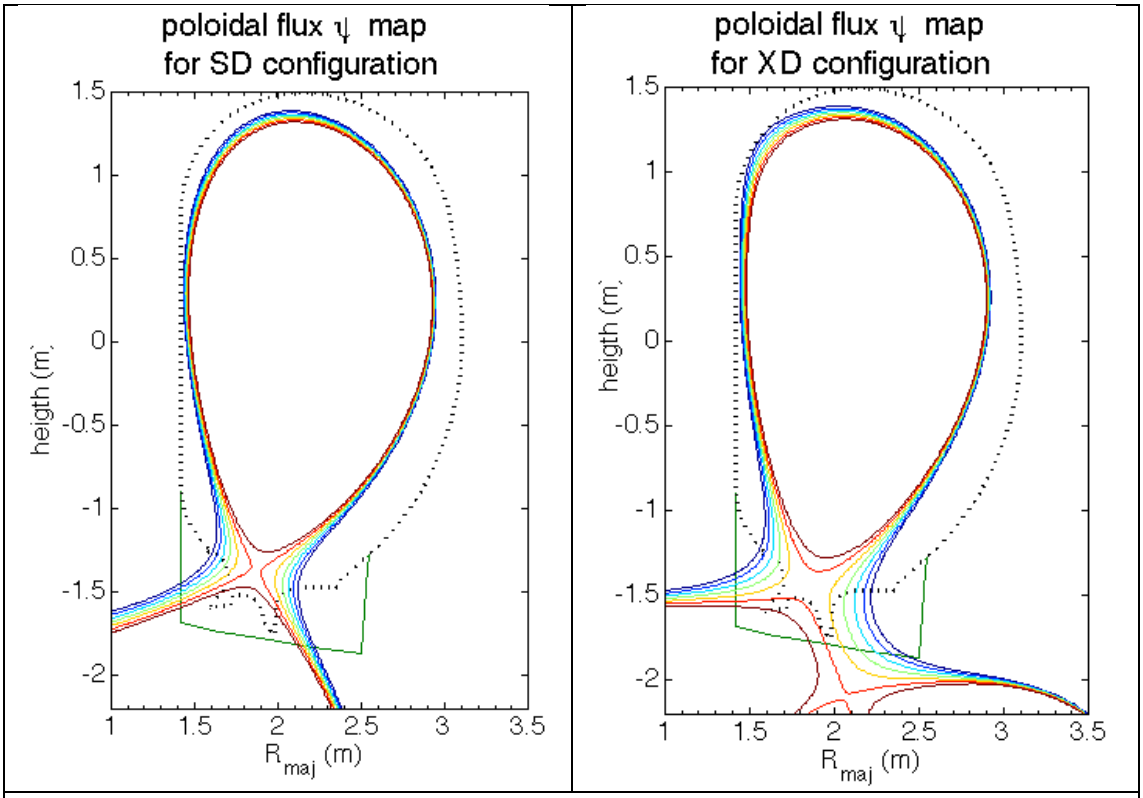

Figure 1 - Computed equilibria of SD (left) and XD (right). The wall shape suitable for SD is shown with a dashed black curve. The shape assumed for all configuration assumed in this paper is show as a green continuous line

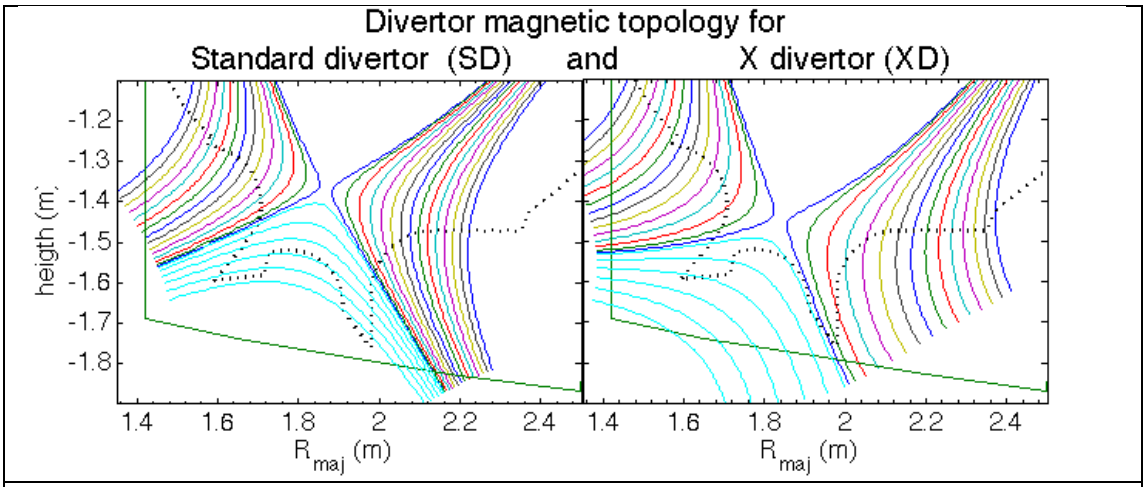

Figure 2 - Details of the divertor region for the computed equilibria of SD (left) and XD (right)

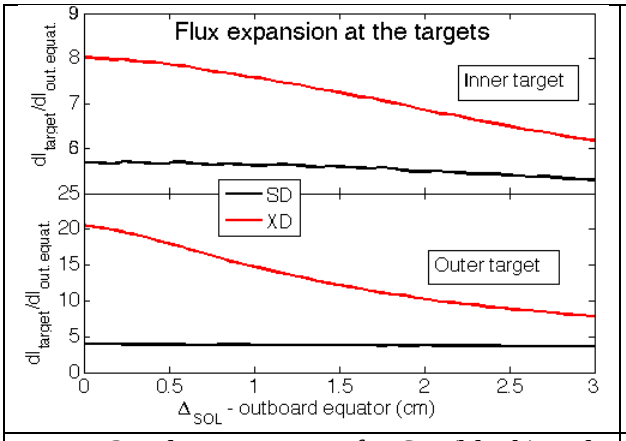

Figure 3 - Flux expansion for SD (black) and XD on both targets

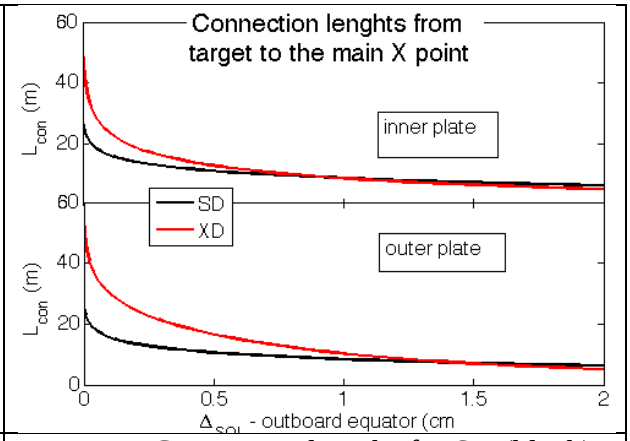

Figure 4 - Connection lengths for SD (black) and XD on both divertor legs

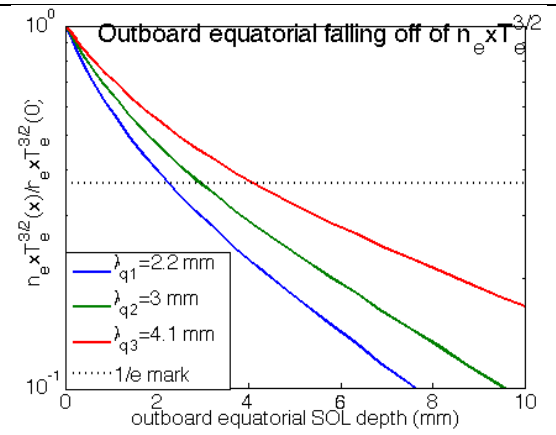

Figure 5 - Radial fall-off of $n_e \times T_e^{3/2}$ on the outer equator for the SD, well attached case for the three couples of cross-field diffusion coefficients given in the text

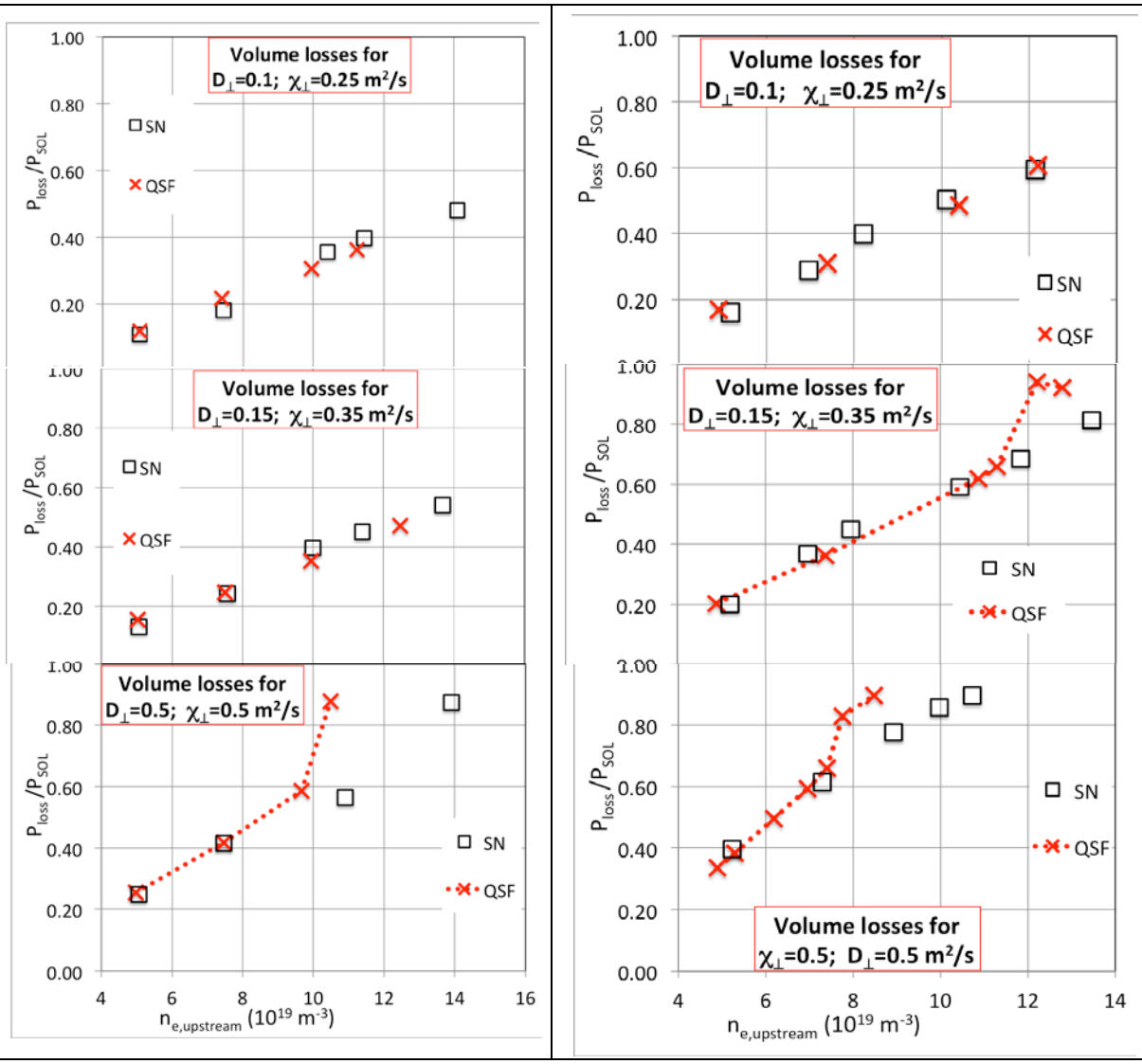

Figure 6 - Total volume power losses versus the upstream separatrix density for the three different couples of cross-field transport and for two different power entering the SOL, namely P_{SOL}=35 MW (left column) and P_{SOL}= 25 MW (right column)

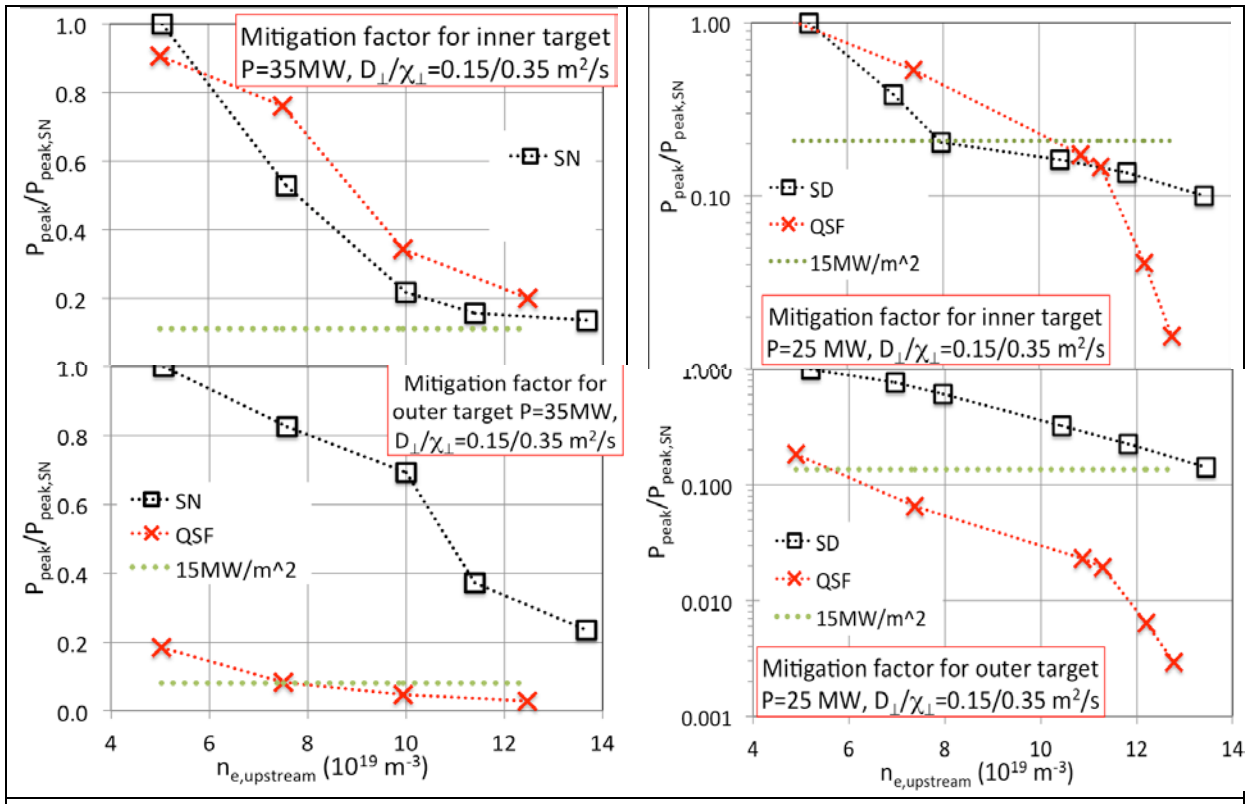

Figure 7 - Mitigation factor for the peak load versus the upstream separatrix density couples of cross-field transport and for two different power entering the SOL, namely P_{SOL}=35 MW (left column) and P_{SOL}= 25 MW (right column)

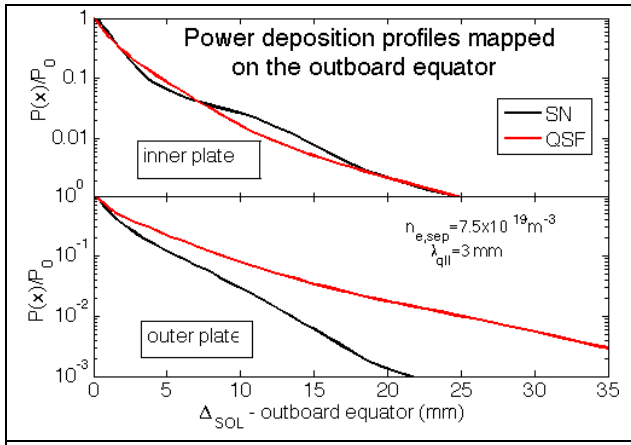

Figure 8 - Normalized power deposition profiles on the inner and outer target, respectively top and bottom frame, mapped versus the outboard equatorial distance

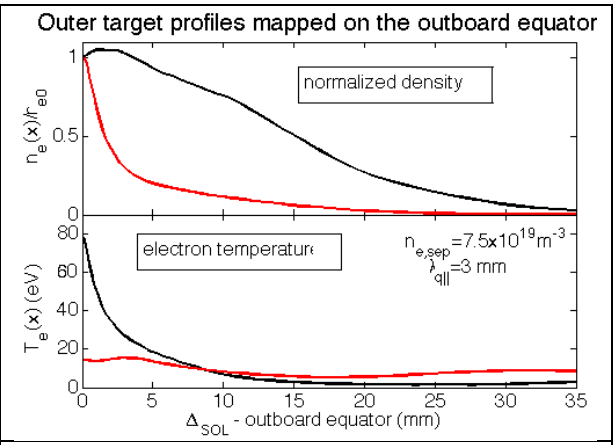

Figure 9 - profiles on the outer target of density, normalized to the peak (top) and electron temperature (bottom) for the same case considered in the previous figure

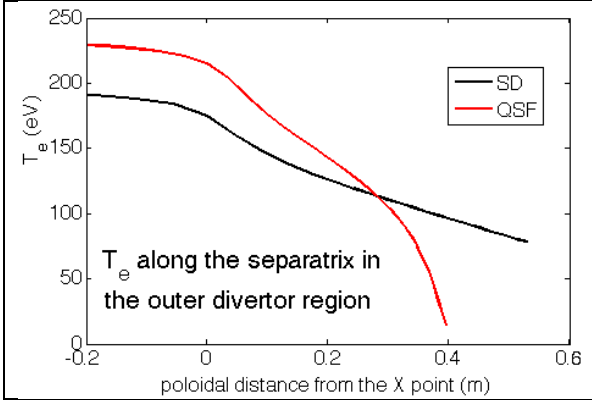

Figure 10 - Variation of the electron temperature along the separatrix from the main X point to target for SD and QSF configurations. The parameters of the simulations are the same of the previous figures.

Conclusions

The possible scenarios at full power of the proposed device have been analyzed for the aspect of safely handling the power to be exhausted on the divertor targets. In this conceptual design phase the computational tools have been chosen mainly on the basis of their simplicity and rapidity. This allows outlining in a reasonable time the general features of the problem and giving indications to a subsequent more rigorous analysis. The code COREDIV was used for a preliminary self-consistent description of the coupled edge-core system. Subsequently, a more punctual analysis has been carried out on the SOL. Only the steady state, where ELMs are neglected, is considered and focus is cast on the highest heat load cases, when no impurity is injected to sustain the radiative dissipation of the injected power. In this case the results, indicate that the peak loads are not sustainable in SD configuration at low density, are border-line for the reference case - crucial then becomes the plates tilting - and reach a manageable value at high density.

The difference with COREDIV that predicts for all scenarios quite similar loads is essentially in the fact that TECXY takes into account the actual magnetic topology and then better estimates the volume losses inside the SOL. Therefore, the possible scenarios at full power and a bit reduced one of the proposed DTT have been analysed by TECXY with the main aim to elucidate differences in the power deposition issues between the standard divertor configuration and the advanced one, which can be classified either as an expanded divertor, or a quasi-snow flake. The still lacking final design of the divertor does not make very meaningful using complex codes that would need the details of the divertor layout, namely shape, baffles, pump and so on, in order to be actually reliable. Furthermore, these tools are quite unpractical for exploring the possible working parameter space, due to their quite long running times. We have identified the 2D code TECXY as a good compromise for this phase of the project and the most appropriate tool for our purposes. As pointed out before, the simplified neutral treatment of the neutral dynamics does not allow to describe properly a situation where the role of the neutrals is dominant, as in detached conditions, but still allows to identify the conditions where such detachment is approached. Further, the lack of a final design has led us to consider a conventional, very simplified, divertor geometry with the targets perpendicular to the poloidal field line. Therefore the absolute numbers for the loads are not fully meaningful, whereas their variation with the main plasma parameters can be reliably traced. Furthermore we limited at this stage our analysis to the impurity non-seeded case, since this situation is the most interesting one for the figure of merit P/R that can even exceed the ITER value.

The main outcome of this study is that in term of global parameters little difference exists between the two configurations for low working densities. The reason is identified in the fact that the topology modifications occur in region where the dissipative processes, radiation inelastic collisions etc., are rather negligible to be enhanced at significant level.
The situation shows different at higher density where the QSF (or XD) seems indeed to favour detached operations and strongly radiating regimes. This trend is reinforced by lowering the power entering the SOL and by faster cross-field diffusion. These very important regimes seem to be reachable by the advanced configurations of DTT, for some appropriate choice of the working parameters. Indeed, it is to stress that comparing the two configurations for the same value of separatrix density may be not fully consistent, since for a fixed volume average density, we expect higher edge density for QSF, which goes in the right direction towards detachment. While the detailed mechanism for this fact to occur is still matter of investigation, it appears that a crucial role is played by the enhanced cross filed diffusion of the power channel induced by increasing the connection lengths. The temperature suffers a large radial broadening that can drop its value at target to values high enough to enhance significantly all the volume losses.
In the regimes far from detachment the flux expansion plus the T_e spreading just described are quite promising for a safe operation of the targets below the technological limits for the power handling for QSF, especially at moderate/high density. Conversely it seems problematic the operation with SD without some independent mechanism to improve radiation, e.g. impurity seeding. However a final assessment on this point clearly claims for a definition of the plate geometry.

We can then expect that further optimization of the position of the secondary nulls on both legs could significantly improve the divertor characteristics from the exhaust point of view.

Acknowledgements

This work has been carried out within the framework of the EUROfusion Consortium and has received funding from the Euratom research and training programme 2014-2018 under grant agreement No 633053. The views and opinions expressed herein do not necessarily reflect those of the European Commission. This scientific work was financed within the Polish framework of the scientific financial resources in 2016 allocated for realization of the international co-financed project.

REFERENCES

[1] R. Stankiewicz, R. Zagórski, J. Nucl. Mater., **313-316** (2003) 899.
[2] J. G. Cordey et al., Plasma Phys. Control. Fusion **39** (1997) B115–B127
[3] R. Zagórski et al., Contrib. Plasma Phys. **48** 179-84 and J. Nucl. Mater. **390-391** 404
[4] R. Zagórski et al., Nucl. Fusion **55** (2015) 053032 (9pp) doi:10.1088/0029-5515/55/5/053032
[5] V. Pericoli Ridolfini et al., Fus. Eng. Des **88** (2013) 1677-1681
[6] T. Eich et al., Phys. Rev. Lett. **107** (2011) 215001
[7] R. Zagórski and H. Gerhauser, Phys. Scr.**70** (Part 2/3) 173 (2004)
[8] G. Calabrò et al., Nucl. Fusion **V. 55**. **No. 8** (2015) 083005
[9] V. Pericoli Ridolfini et al., J. Nucl. Mat., **V. 438**, , pp. S414-S417 July 2013 doi: 10.1016/j.jnucmat.2013.01.083

[10] T. Eich et al., Phys. Rev. Lett.107 (2011) 215001 and Nucl. Fus., 53 093031 (2013)
[11] M. Leigheb, V. Pericoli Ridolfini, R. Zagórski, J. Nucl. Mat., **V. 241-243**, p. 914-918, doi: 10.1016/S0022-3115(97)80165-1
[12] P. Stangeby, The Plasma Boundary of Magnetic Fusion Devices, ISBN 0750305592, IoP (2000)